SCIENCE CHINA
Information Sciences

• RESEARCH PAPER •

January 2020, Vol. 63 112204:1–112204:12
https://doi.org/10.1007/s11432-019-9896-2

Dual-mode predictive control of a rotor suspension system

Yue WU[1,2], Gui-Ping REN[1,2] & Hai-Tao ZHANG[1,2*]

[1]*Key Laboratory of Image Processing and Intelligent Control, School of Artificial Intelligence and Automation, Huazhong University of Science and Technology, Wuhan 430074, China;*
[2]*State Key Laboratory of Digital Manufacturing Equipments and Technology, Wuhan 430074, China*

Received 21 February 2019/Revised 8 April 2019/Accepted 29 April 2019/Published online 25 December 2019

Abstract Rotor active magnetic bearing (rotor-AMB) systems are frequently used to alleviate vibrations for various applications such as in national defense, manufacturing industries, IC production, and aerospace engineering. One obstacle to improve machining efficiency and quality is the open-loop instability of rotor-AMB systems during the machining process. We built a closed-loop processing platform using a spindle rotor installed with AMBs and thereby developed a rotor-AMB suspension system embedded with a dual-mode predictive controller (DMPC). The performance of the system is thus substantially improved. In the proposed DMPC, both model-based prediction and receding horizon optimization are utilized to guarantee the closed-loop stability of the rotor-AMB suspension systems with input constraints. Finally, the effectiveness and superiority of the proposed method are examined through substantial levitation experiments on a machining platform with installed AMBs.

Keywords dual-mode predictive control, system identification, optimization control, model predictive control, suspension control

Citation Wu Y, Ren G-P, Zhang H-T. Dual-mode predictive control of a rotor suspension system. Sci China Inf Sci, 2020, 63(1): 112204, https://doi.org/10.1007/s11432-019-9896-2

1 Introduction

In recent decades, active magnetic bearings (AMBs) and electromagnetic levitation techniques have been widely used in a variety of industrial rotating machineries including compressors, spindle turbines, and turbomachinery [1,2]. Compared with conventional rolling element bearings for machining processes, the virtues of AMBs lie in their greater abilities of adjustable damping and stiffness, high rotor speeds and small rotor vibrations [3,4].

Unfortunately, the AMB system is a typical mechatronics system exhibiting open-loop instability characteristics [5]. Therefore, it is essential to develop niche controllers to stabilize a closed-loop rotor-AMB system. Many efforts have been devoted to the design of controllers to attenuate vibrations. In [6], a μ-synthesis control approach was developed to suppress external disturbances for a flexible rotor-AMB system. Sivrioglu [7] proposed an output-type adaptive back-stepping controller for zero-bias current AMB systems, which overcomes the nonlinear dynamics and parametric uncertainties, reduces the power loss, and improves the control performance. In [8], AMBs were used to levitate the elevation axis of an electro-optical sight system in a moving vehicle, and the effect of model uncertainties and disturbances was reduced by a designed sliding mode control. Furthermore, in [9], a multivariable H_∞ controller was designed for a rotor-AMB system involving an uncertain bearing stiffness and rotor speed. With the

* Corresponding author (email: zht@hust.edu.cn)

H_∞ controller, the rotor vibrations were effectively mitigated. Dong et al. [10] developed two types of adaptive back-stepping control for an AMB system with external disturbances and uncertainties, and they achieved excellent control performance for restraining disturbance. Pesch et al. [11] designed a new method for tooltip tracking control of a spindle with AMBs and confirmed the reference tracking accuracy and the disturbance rejection ability by using a μ-synthesis model-based robust controller. Kandil et al. [12] proposed twisting and suboptimal algorithms based on second-order sliding mode control for AMB systems with model uncertainties and time-varying harmonic disturbances. These algorithms reduced the maximum rotor deviation compared with the traditional linear method. Xie et al. [13] reported a 3-loop control structure for an active magnetic control system in a labyrinth piston compressor, which improves the running performance by suppressing the eccentricity of the piston rod.

It has been noted that in engineering applications of control systems, input constraints ubiquitously exist due to the output limits of the drivers/actuators [14, 15]. Moreover, input constraints have not been considered but cannot be ignored in the analysis and application of rotor-AMB systems. However, thus far, due to the nonlinearity of AMB systems, and the strong coupling between the bearings and the rotor, few researchers have taken input constraints into consideration. To address this challenge, in this paper, a novel active controller based on a model predictive control (MPC) technique is developed to stabilize a constrained AMB system. The MPC and dual-mode predictive control (DMPC) techniques are common control strategies in manufacturing industries [16–19] because of their capability to overcome nonlinearities and system uncertainties and to deal with constraints [20–22]. Basically, in the framework of MPC, with the system dynamics identified by an internal model, an optimal control input trajectory can be obtained by solving the receding horizon optimization problem online, which minimizes a given performance index [23–25]. Therefore, when the MPC technique is applied to a machining process, it is expected that an optimal control input trajectory can be determined. For instance, in [26], an MPC scheme was developed to eliminate the chatter effect and improve the stability lobe diagram.

The present work provides the following contributions. (i) The accessible operational region is effectively expanded based on a DMPC scheme [27, 28]. More precisely, using the LaSalle invariant set theorem [29], a rotor-AMB system with input constraints on the actuators is stabilized. (ii) The online computational load is reduced for the AMB system. (iii) The rotor vibrations excited by random external disturbances are mitigated. Meanwhile, a detailed parameter design scheme is given based on a systematic technical analysis. Hence, the present work is an attempt to pave the way from theoretical control algorithms to actual industrial applications of rotor AMBs.

The remainder of this paper is organized as follows. The architecture of the rotor-AMB platform is introduced, and the dynamics of the internal model are presented in Section 2. In Section 3, the DMPC technique is described. In Section 4, an experimental case study on the proposed rotor-AMB platform is conducted to verify the effectiveness of the proposed controller. Finally, Section 5 presents the conclusion of this work.

The following notations are utilized in this paper. $\mathbb{R}$ denotes a real number set, and the matrices $\mathbf{0}$ and $\boldsymbol{I}$ represent zero and identity matrices with compatible dimensions, respectively. The symbols "$\prec$ / $\preceq$" and "$\succ$ / $\succeq$" denote negative/semi-negative and positive/semi-positive definiteness for square matrices, respectively. The notation $\widehat{\boldsymbol{x}}(k+i|k)$ denotes the predictive value at the $(k+i)$-th step according to the k-th step information for $\boldsymbol{x}$. The Euclidean 2-norm is expressed by the notation $\|\cdot\|_2$.

2 Architecture and model of the rotor-AMB system

The experimental platform and structure of the rotor-AMB system are presented in Figure 1 with a magnified image of the rotor. The architecture of the rotor-AMB control system is illustrated in Figure 2. More precisely, the front and back vibrations of the rotor are detected by the front (b_3) and back (b_4) displacement sensors, respectively. The displacement signals are regulated by a signal processing circuit a_5, where low-pass filters are embedded to filter undesired high-frequency noise; then, the signals are transferred to controller a_2, which is based on a high-capability FPGA with a 50-MHz crystal oscillator.

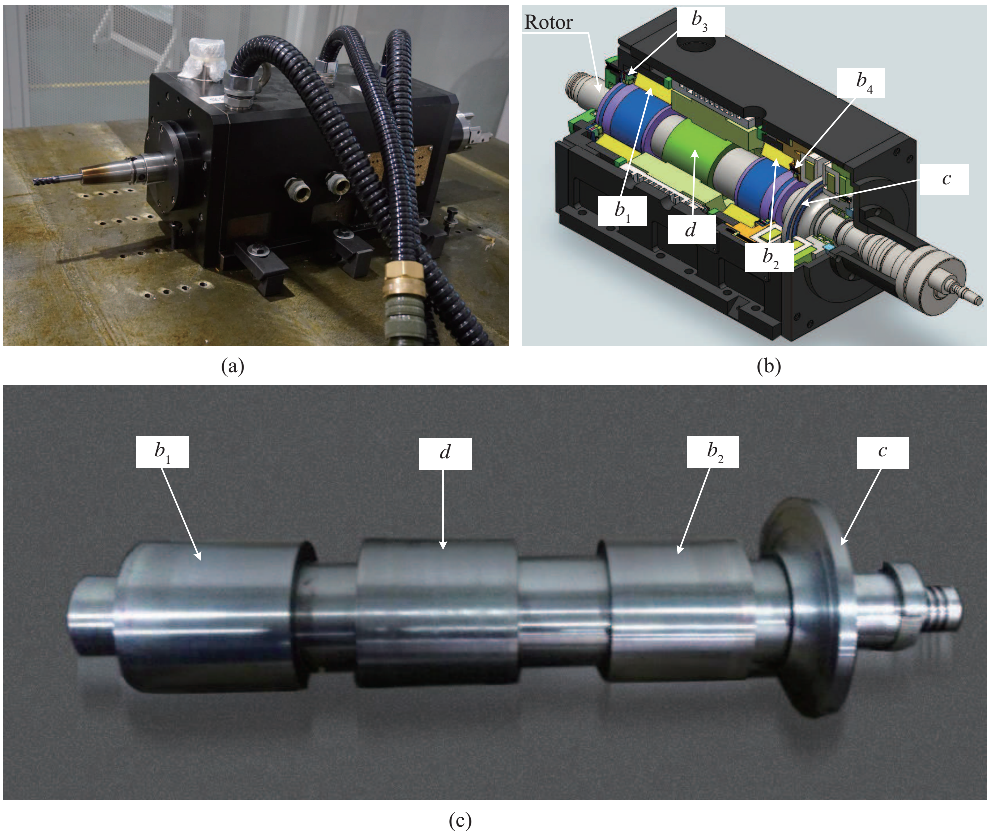

Figure 1 (Color online) (a) Spindle with AMBs. (b) Structure of the spindle with installed AMBs. b_1: front bearing; b_2: back bearing; b_3: front position sensors; b_4: back position sensors; c: axial bearing; d: motor. (c) Magnified image of the rotor.

Subsequently, according to the calculated control signals, the amplifiers a_3 and a_4 drive the coils via an H-bridge circuit and a proportion integration (PI) current controller. Finally, the combined coil currents generate adjustable magnetic forces to support rotor and vibration mitigation.

The dynamic coupling of the axial and radial rotor motions is sufficiently weak; these motions are generally assumed to be independent of each other, and only radial dynamics are considered. Meanwhile, the cross-coupling forces excited by the front and back AMBs are ignored. It should be mentioned that the rotor is installed vertically on the machine tool; in this case, we do not have to consider gravity for the radial AMBs. Hence, the simplified rotor-AMB system dynamic is described as follows:

$$\boldsymbol{M}_l \ddot{\boldsymbol{q}}_l(t) = \boldsymbol{F}_l(t), \tag{1}$$

where $\boldsymbol{M}_l \in \mathbb{R}^{2\times 2}$ and $\boldsymbol{q}_l(t) := [q_{l,x}(t), q_{l,y}(t)]^{\mathrm{T}}$ are the system mass and perturbation displacement vector for the rotor, respectively. Here, $l = f, b$ denotes the front and back AMBs, and the actuator force $\boldsymbol{F}_l(t) := [f_{l,x}(t), f_{l,y}(t)]^{\mathrm{T}}$ satisfies the following [5]:

$$f_{l,j}(t) = \beta_{l,j}\left(\frac{(i_0 + i_{l,j1}(t))^2}{(q_0 - q_{l,j}(t))^2} - \frac{(i_0 - i_{l,j2}(t))^2}{(q_0 + q_{l,j}(t))^2}\right),$$

where $\beta_{l,j} := \mu\zeta N^2$ are the inherent parameters of the AMB, ζ represents the pole area, μ is the air permeability of vacuum $\mu \approx \mu_0 = 4\pi\mathrm{e}^{-7}$ Vs/Am, i_0 is the bias current with $i_{l,j1}(t)$ and $i_{l,j2}(t)$ as the input currents of the actuator, $j = x, y$, and q_0 denotes the corresponding nominal gap length. Note that the displacement $\boldsymbol{q}_l(t)$ is usually much less than q_0.

Next, the actuator force model can be linearized at the origin ($i_{l,j1}(t) = 0$, $i_{l,j2}(t) = 0$, $q_{l,j}(t) = 0$) as follows:

$$\boldsymbol{F}_l(t) = \boldsymbol{\Gamma}_{l1,i}\boldsymbol{i}_{l1}(t) + \boldsymbol{\Gamma}_{l2,i}\boldsymbol{i}_{l2}(t) + \boldsymbol{\Gamma}_{l,q}\boldsymbol{q}_l(t), \tag{2}$$

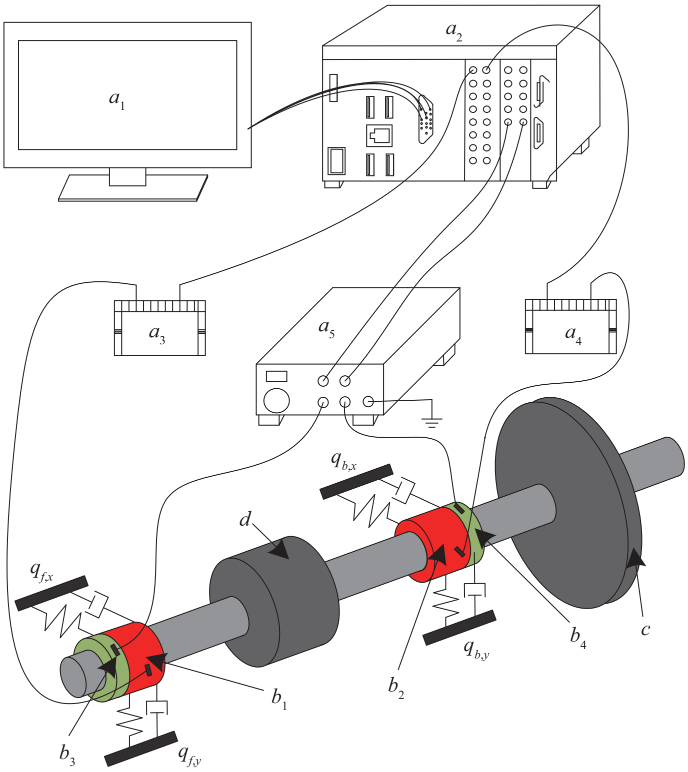

Figure 2 (Color online) Architecture of the control system of the rotor-AMB platform displayed in Figure 1. a_1: monitor; a_2: controller; a_3 and a_4: power amplifiers; a_5: displacement amplifiers and filters.

where $\boldsymbol{\Gamma}_{l1,i} := \mathrm{diag}(2i_0\beta_{l,x}/q_0^2, 2i_0\beta_{l,y}/q_0^2)$, $\boldsymbol{\Gamma}_{l2,i} := \mathrm{diag}(-2i_0\beta_{l,x}/q_0^2, -2i_0\beta_{l,y}/q_0^2)$, and $\boldsymbol{\Gamma}_{l,q} := \mathrm{diag}(4\beta_{l,x}i_0^2/q_0^3, 4\beta_{l,y}i_0^2/q_0^3)$ denote linearized coefficients. $\boldsymbol{i}_{l1}(t) = [i_{l,x1}(t), i_{l,y1}(t)]^{\mathrm{T}}$ and $\boldsymbol{i}_{l2}(t) = [i_{l,x2}(t), i_{l,y2}(t)]^{\mathrm{T}}$ represent the control laws (i.e., the input currents of the actuator).

State-space descriptions of the unidirectional magnetic coil power amplifiers with a PI current loop can be given as follows:

$$\dot{\boldsymbol{x}}_{l,jn}(t) = \boldsymbol{A}_{l,jn}\boldsymbol{x}_{l,jn}(t) + \boldsymbol{B}_{l,jn}u_{l,j}(t), \quad i_{l,jn}(t) = \boldsymbol{C}_{l,jn}\boldsymbol{x}_{l,jn}(t), \tag{3}$$

where $n = 1, 2$, $\boldsymbol{A}_{l,jn} = [0, 1; -\omega_{l,jn}^2, -\zeta_{l,jn}^2\omega_{l,jn}^2]$, $\boldsymbol{B}_{l,jn} = [0, 1]^{\mathrm{T}}$, $\boldsymbol{C}_{l,jn} = [\omega_{l,jn}^2, 0]$, and $u_{l,j}(t)$ is the control voltage.

The dynamics of the linear displacement amplifiers and third-order low-pass filters are as follows:

$$\dot{\boldsymbol{x}}_{l,j}(t) = \boldsymbol{A}_{l,j}\boldsymbol{x}_{l,j}(t) + \boldsymbol{B}_{l,j}q_{l,j}(t), \quad \overline{q}_{l,j}(t) = \boldsymbol{C}_{l,j}\boldsymbol{x}_{l,j}(t), \tag{4}$$

where $\boldsymbol{A}_{l,j} = [0, 1, 0; 0, 0, 1; -a_{l,j1}, -a_{l,j2}, -a_{l,j3}]$, $\boldsymbol{B}_{l,j} = [0, 0, 1]^{\mathrm{T}}$, $\boldsymbol{C}_{l,j} = [a_{l,j1}, 0, 0]$, and $\overline{q}_{l,j}(t)$ are the corresponding output signals.

Thereby, the dynamics of the rotor-AMB system with the corresponding power amplifiers and position filters are described as follows:

$$\dot{\boldsymbol{x}}_q(t) = \boldsymbol{A}_q\boldsymbol{x}_q(t) + \boldsymbol{B}_q\boldsymbol{u}_q(t), \quad \overline{\boldsymbol{q}}(t) = \boldsymbol{C}_q\boldsymbol{x}_q(t), \tag{5}$$

with $\boldsymbol{x}_q(t) \in \mathbb{R}^{36}$, $\boldsymbol{u}_q(t) \in \mathbb{R}^4$, $\overline{\boldsymbol{q}}(t) \in \mathbb{R}^4$,

$$\begin{aligned}
&\boldsymbol{A}_q = [\boldsymbol{A}_{11}, \boldsymbol{A}_{12}, \boldsymbol{0}_{12\times16}; \boldsymbol{0}_{8\times12}, \boldsymbol{A}_{22}, \boldsymbol{A}_{23}; \boldsymbol{0}_{16\times20}, \boldsymbol{A}_{33}], \quad \boldsymbol{A}_{11} = \mathrm{diag}(\boldsymbol{A}_{f,x}, \boldsymbol{A}_{f,y}, \boldsymbol{A}_{b,x}, \boldsymbol{A}_{b,y}),\\
&\boldsymbol{A}_{12} = [\overline{\boldsymbol{B}}_f\overline{\boldsymbol{C}}_f, \boldsymbol{0}_{6\times4}; \boldsymbol{0}_{6\times4}, \overline{\boldsymbol{B}}_b\overline{\boldsymbol{C}}_b], \quad \overline{\boldsymbol{B}}_l = [\boldsymbol{B}_{l,x}^{\mathrm{T}}, \boldsymbol{0}_{1\times3}; \boldsymbol{0}_{1\times3}, \boldsymbol{B}_{l,y}^{\mathrm{T}}]^{\mathrm{T}}, \quad \overline{\boldsymbol{C}}_l = [\boldsymbol{I}_2, \boldsymbol{0}_2],\\
&\boldsymbol{A}_{22} = \mathrm{diag}(\overline{\boldsymbol{A}}_f, \overline{\boldsymbol{A}}_b,), \quad \overline{\boldsymbol{A}}_l = [\boldsymbol{0}_2, \boldsymbol{I}_2; \boldsymbol{M}_p^{-1}\boldsymbol{\Gamma}_{l,q}, \boldsymbol{0}_2],\\
&\boldsymbol{A}_{23} = [\widetilde{\boldsymbol{B}}_{f1}\widetilde{\boldsymbol{C}}_{f1}, \widetilde{\boldsymbol{B}}_{f2}\widetilde{\boldsymbol{C}}_{f2}, \boldsymbol{0}_{8\times16}; \boldsymbol{0}_{8\times16}, \widetilde{\boldsymbol{B}}_{b1}\widetilde{\boldsymbol{C}}_{b1}, \widetilde{\boldsymbol{B}}_{b2}\widetilde{\boldsymbol{C}}_{b2}],
\end{aligned}$$

Table 1 Parameters for two axial AMBs in the spindle

Data	Value	Units
AMB mass $M_{f,b}$	diag(8,8), diag(6,6)	kg
Coil turns $N_{f,b}$	180, 180	–
Pole area $\zeta_{f,b}$	850, 612	mm^2
Nominal gap length q_0	0.50	mm
Backup bearing gap R_0	0.25	mm
Bias current I_0	0.5	A

$$
\begin{aligned}
&\widetilde{\boldsymbol{B}}_{ln} = [\boldsymbol{0}_2, \boldsymbol{M}_p^{-1}\boldsymbol{\Gamma}_{ln,i}]^{\mathrm{T}}, \quad \widetilde{\boldsymbol{C}}_{ln} = [\boldsymbol{C}_{l,xn}, \boldsymbol{0}_{1\times 2}; \boldsymbol{0}_{1\times 2}, \boldsymbol{C}_{l,yn}],\\
&\boldsymbol{A}_{33} = \mathrm{diag}(\boldsymbol{A}_{f,x1}, \boldsymbol{A}_{f,y1}, \boldsymbol{A}_{f,x2}, \boldsymbol{A}_{f,y2}, \boldsymbol{A}_{b,x1}, \boldsymbol{A}_{b,y1}, \boldsymbol{A}_{b,x2}, \boldsymbol{A}_{b,y2}),\\
&\boldsymbol{B}_q = [\boldsymbol{0}_{1\times 20}, \boldsymbol{B}_{f,x1}^{\mathrm{T}}, \boldsymbol{0}_{1\times 2}, \boldsymbol{B}_{f,x2}, \boldsymbol{0}_{1\times 10}; \boldsymbol{0}_{1\times 22}, \boldsymbol{B}_{f,y1}^{\mathrm{T}}, \boldsymbol{0}_{1\times 2}, \boldsymbol{B}_{f,y2}, \boldsymbol{0}_{1\times 8};\\
&\qquad \boldsymbol{0}_{1\times 28}, \boldsymbol{B}_{b,x1}^{\mathrm{T}}, \boldsymbol{0}_{1\times 2}, \boldsymbol{B}_{b,x2}, \boldsymbol{0}_{1\times 2}; \boldsymbol{0}_{1\times 30}, \boldsymbol{B}_{b,x1}^{\mathrm{T}}, \boldsymbol{0}_{1\times 2}, \boldsymbol{B}_{b,x2}]^{\mathrm{T}},\\
&\boldsymbol{C}_q = [\boldsymbol{C}_{f,x}, \boldsymbol{0}_{1\times 33}; \boldsymbol{0}_{1\times 3}, \boldsymbol{C}_{f,y}, \boldsymbol{0}_{1\times 30}; \boldsymbol{0}_{1\times 6}, \boldsymbol{C}_{b,x}, \boldsymbol{0}_{1\times 27}; \boldsymbol{0}_{1\times 9}, \boldsymbol{C}_{b,y}, \boldsymbol{0}_{1\times 24}],\\
&\boldsymbol{u}_q(t) := [u_{f,x}(t), u_{f,y}(t), u_{b,x}(t), u_{b,y}(t)]^{\mathrm{T}},\\
&\overline{\boldsymbol{q}}(t) := [\overline{q}_{f,x}(t), \overline{q}_{f,y}(t), \overline{q}_{b,x}(t), \overline{q}_{b,y}(t)]^{\mathrm{T}}.
\end{aligned}
$$

3 Controller design for the rotor-AMB system

The system (5) can be discretized as follows:

$$
\boldsymbol{x}(k+1) = \boldsymbol{A}\boldsymbol{x}(k) + \boldsymbol{B}\boldsymbol{u}(k), \quad \boldsymbol{q}(k+1) = \boldsymbol{C}\boldsymbol{x}(k+1), \tag{6}
$$

with $\boldsymbol{x}(k) \in \mathbb{R}^m$, $\boldsymbol{u}(k) \in \mathbb{R}^p$, $\boldsymbol{q}(k) \in \mathbb{R}^q$, $m = 36$, $p = 4$, $q = 4$, sampling time $T_s = 0.0001$ s.

It is straightforward to demonstrate that the discrete-time system model (6) is unstable, as some eigenvalues of $\boldsymbol{A}$ (see model parameters in Table 1) are outside the unit circle. Furthermore, system (6) is a complex high-order MIMO system, rendering the development of a stable closed-loop controller difficult. To this end, a DMPC strategy is proposed to stabilize the rotor-AMB system.

Note that system (6) is stabilizable, and there exists a matrix $\boldsymbol{K}$ such that $\boldsymbol{\Phi} = \boldsymbol{A} + \boldsymbol{B}\boldsymbol{K}$ is a Hurwitz matrix. First, an optimal matrix $\boldsymbol{K}$ is identified for the design of the DMPC based on the linear quadratic regulator (LQR) algorithm while ensuring that $\boldsymbol{\Phi}$ is a Hurwitz matrix and the cost function

$$
J = \sum_{k=0}^{\infty} \left(\boldsymbol{x}^{\mathrm{T}}(k)\boldsymbol{Q}\boldsymbol{x}(k) + \boldsymbol{u}^{\mathrm{T}}(k)\boldsymbol{R}\boldsymbol{u}(k)\right) \tag{7}
$$

is minimized. Here, the weighting matrices $\boldsymbol{Q} \in \mathbb{R}^m$ and $\boldsymbol{R} \in \mathbb{R}^p$ are positive definite. For simplicity, these matrices are set as $\boldsymbol{Q} = \boldsymbol{I}$ and $\boldsymbol{R} = \sigma\boldsymbol{I}$ with $\sigma \geqslant 0$.

Because rotor-AMB system (6) is observable, we design a state observer as

$$
\begin{aligned}
&\widehat{\boldsymbol{x}}(k+1) = \boldsymbol{A}\widehat{\boldsymbol{x}}(k) + \boldsymbol{B}\boldsymbol{u}(k) + \boldsymbol{L}_1\boldsymbol{C}\widetilde{\boldsymbol{x}}(k),\\
&\boldsymbol{q}_s(k+1) = \boldsymbol{C}\widehat{\boldsymbol{x}}(k+1),\\
&\widetilde{\boldsymbol{x}}(k+1) = \boldsymbol{\Omega}\widetilde{\boldsymbol{x}}(k),
\end{aligned} \tag{8}
$$

in which the state $\widehat{\boldsymbol{x}}(k)$ is introduced to estimate $\boldsymbol{x}(k)$ and $\boldsymbol{\Omega} = \boldsymbol{A} - \boldsymbol{L}_1\boldsymbol{C}$ is a Hurwitz matrix. We assume that the state estimation error is $\widetilde{\boldsymbol{x}}(k) := \boldsymbol{x}(k) - \widehat{\boldsymbol{x}}(k)$.

We can now design a DMPC such that the state $\boldsymbol{x}(k)$ converges to the origin. For this purpose, we design the controller as follows:

$$\widehat{\boldsymbol{u}}(k|k) = \boldsymbol{K}\widehat{\boldsymbol{x}}(k|k) + \boldsymbol{W}\widehat{\boldsymbol{\xi}}(k|k) \tag{9}$$

with $\widehat{\boldsymbol{u}}(k|k) = \boldsymbol{u}(k)$, $\widehat{\boldsymbol{x}}(k|k) = \boldsymbol{x}(k)$, $\widehat{\boldsymbol{\xi}}(k|k) = \boldsymbol{\xi}(k) := [\boldsymbol{\epsilon}(k)^{\mathrm{T}}, \ldots, \widehat{\boldsymbol{\epsilon}}(k+M-1|k)^{\mathrm{T}}]^{\mathrm{T}}$, and $M \geqslant 1$ as the predictive horizon. Matrix $\boldsymbol{W}$ selects the first p entries of $\boldsymbol{\xi}(k)$. The perturbation term $\widehat{\boldsymbol{\xi}}(k|k)$ denotes additional degrees of design freedom to ensure that $\boldsymbol{x}(k)$ is backed into the stability region [30]. This approach enlarges the feasible initial state domain that guarantees effective control (9). Furthermore, we design $\widehat{\boldsymbol{\xi}}(k+i|k)$ as follows:

$$\widehat{\boldsymbol{\xi}}(k+i|k) = \boldsymbol{L}_2\widehat{\boldsymbol{\xi}}(k+i-1|k), \quad i = 1, 2, \ldots M, \tag{10}$$

with

$$\boldsymbol{L}_2 = \begin{bmatrix} \boldsymbol{0} & \boldsymbol{I}_{(M-1)p} \\ \boldsymbol{0} & \boldsymbol{0}^{\mathrm{T}} \end{bmatrix}_{Mp\times Mp}.$$

The proposed controller is a dual-mode controller because $\widehat{\boldsymbol{\xi}}(k+i|k)$ vanishes to zero within M steps and then the controller becomes $\boldsymbol{u} = \boldsymbol{K}\widehat{\boldsymbol{x}}$, which is an LQR controller.

To facilitate the design of the controller (9), an invariant set $\mathcal{S}_x$ for $\widehat{\boldsymbol{x}}(k)$ is defined as follows:

$$\mathcal{S}_x := \{\widehat{\boldsymbol{x}}(k)|\widehat{\boldsymbol{x}}^{\mathrm{T}}(k)\boldsymbol{P}_x\widehat{\boldsymbol{x}}(k) \leqslant 1\}, \tag{11}$$

where matrix $\boldsymbol{P}_x$ is positive-definite. A hard input constraint (e.g., actuator power limitation) is considered, i.e., $|\widehat{u}_j(k+i|k)| \leqslant \overline{u}$ with $\overline{u} > 0$, $j = 1, 2, \ldots p$ and u_j as the j-th element in the vector $\widehat{\boldsymbol{u}}$, which is often encountered in rotor-AMB machining processes. We substitute Eq. (9) into the observer (8), which yields

$$\widehat{\boldsymbol{z}}(k+i|k) = \boldsymbol{\Theta}\widehat{\boldsymbol{z}}(k+i-1|k) + \boldsymbol{\Psi}\widetilde{\boldsymbol{x}}(k), \quad \widehat{\boldsymbol{q}}(k+i|k) = \boldsymbol{C}\widehat{\boldsymbol{x}}(k+i|k), \quad i = 1, \ldots M, \tag{12}$$

where

$$\widehat{\boldsymbol{z}}(k+i|k) := \begin{bmatrix} \widehat{\boldsymbol{x}}(k+i|k) \\ \widehat{\boldsymbol{\xi}}(k+i|k) \end{bmatrix}, \quad \boldsymbol{\Psi} := \begin{bmatrix} \boldsymbol{L}_1\boldsymbol{C} \\ \boldsymbol{0} \end{bmatrix}, \quad \boldsymbol{\Theta} := \begin{bmatrix} \boldsymbol{\Phi} & \boldsymbol{B}\boldsymbol{W} \\ \boldsymbol{0} & \boldsymbol{L}_2 \end{bmatrix}.$$

Moreover, we find

$$\widehat{\boldsymbol{x}}(k+i|k) = \boldsymbol{F}\widehat{\boldsymbol{z}}(k+i|k), \tag{13}$$

where $\boldsymbol{F} = [\boldsymbol{I}_m, \boldsymbol{0}_{m\times Mp}]$.

Two invariant sets, $\mathcal{S}_z$ and $\mathcal{S}_{\widetilde{x}}$, are introduced such that the performance of the system (12) can be evaluated

$$\mathcal{S}_z := \{\boldsymbol{z}(k)|\boldsymbol{z}(k)^{\mathrm{T}}\boldsymbol{P}_z\boldsymbol{z}(k) \leqslant 1\}, \tag{14}$$
$$\mathcal{S}_{\widetilde{x}} := \{\widetilde{\boldsymbol{x}}(k)|\widetilde{\boldsymbol{x}}(k)^{\mathrm{T}}\boldsymbol{P}_{\widetilde{x}}\widetilde{\boldsymbol{x}}(k) \leqslant \widetilde{x}_0\} \;\; (0 < \widetilde{x}_0 < 1), \tag{15}$$

where the matrices $\boldsymbol{P}_z$ and $\boldsymbol{P}_{\widetilde{x}}$ are both positive definite.

The following optimization problem is considered to minimize the perturbation term $\boldsymbol{\xi}(k)$ such that the control cost can be reduced:

$$\min_{\boldsymbol{\xi}(k)} \; J(k) = \boldsymbol{\xi}(k)^{\mathrm{T}}\boldsymbol{\xi}(k) \tag{16}$$
$$\text{s.t. } \|\boldsymbol{P}_z^{1/2}\widehat{\boldsymbol{z}}(k+j|k)\|_2 \leqslant 1.$$

In addition, from Eq. (9), we can rewrite the input constraint as follows:

$$\|\widehat{\boldsymbol{u}}_j(k+i|k)\|_2 = \|\overline{\boldsymbol{K}}_j\widehat{\boldsymbol{z}}(k+i|k)\| \leqslant \overline{u}, \quad i = 0, 1, \ldots M-1, \; j = 1, 2, \ldots p, \tag{17}$$

where $\overline{u} > 0$, $\overline{\boldsymbol{K}}_j$ is the j-th row of $\overline{\boldsymbol{K}}$, $\overline{\boldsymbol{K}} := [\boldsymbol{K}, \boldsymbol{W}]$.

Furthermore, we have the following inequality:

$$\|\overline{\boldsymbol{K}}_j \boldsymbol{z}\| = \|\overline{\boldsymbol{K}}_j \boldsymbol{P}_z^{-1/2} \boldsymbol{P}_z^{1/2} \boldsymbol{z}\| \leqslant \|\overline{\boldsymbol{K}}_j \boldsymbol{P}_z^{-1/2}\|_2 \cdot \|\boldsymbol{P}_z^{1/2} \boldsymbol{z}\|_2 \leqslant \|\overline{\boldsymbol{K}}_j \boldsymbol{P}_z^{-1/2}\|_2.$$

Thereby, if

$$\begin{bmatrix} -\overline{u}^2 & \overline{\boldsymbol{K}}_j \\ \overline{\boldsymbol{K}}_j^{\mathrm{T}} & -\boldsymbol{P}_z \end{bmatrix} \preceq 0, \tag{18}$$

the input constraint (17) always holds.

Before we derive the primary technical result, Assumptions 1–3 are required.

Assumption 1. System (8) is stabilizable and detectable; namely, there exist some matrices $\boldsymbol{L}_1$ and $\boldsymbol{K}$ such that both $\boldsymbol{\Omega}$ and $\boldsymbol{\Phi}$ are Hurwitz matrices.

Assumption 2. There exist $\alpha_1 > 0$, $\alpha_2 > 1$, $0 < \widetilde{x}_0 < 1$, $0 < \alpha_1 \widetilde{x}_0 < 1$, and two symmetric matrices $\boldsymbol{P}_z \succ 0$, $\boldsymbol{P}_{\widetilde{x}} \succ 0$ such that

$$\begin{aligned} &\boldsymbol{\Omega}^{\mathrm{T}} \boldsymbol{P}_{\widetilde{x}} \boldsymbol{\Omega} - \boldsymbol{P}_{\widetilde{x}} \preceq 0, \\ &\alpha_3 \boldsymbol{\Psi}^{\mathrm{T}} \boldsymbol{P}_z \boldsymbol{\Psi} - \alpha_1 \boldsymbol{P}_{\widetilde{x}} \preceq 0, \\ &\alpha_2 \boldsymbol{\Theta}^{\mathrm{T}} \boldsymbol{P}_z \boldsymbol{\Theta} - (1 - \alpha_1 \widetilde{x}_0) \boldsymbol{P}_z \preceq 0, \end{aligned} \tag{19}$$

with $\alpha_3 = 1 + (\alpha_2 - 1)^{-1}$ and $\boldsymbol{\Theta}$ given in (12).

Assumption 3. Eq. (18) holds for $\forall j = 1, 2, \ldots, p$, and the optimization problem (16) and (17) is always solvable.

To stabilize the system (8) and (9), we need symmetric matrices $\boldsymbol{P}_z$ and $\boldsymbol{P}_{\widetilde{x}}$ such that $\mathcal{S}_z$ and $\mathcal{S}_{\widetilde{x}}$ are both invariant (see Eqs. (14) and (15)). Actually, Assumption 2 guarantees that this condition is met. Specifically, if $\widetilde{\boldsymbol{x}}(k+i)^{\mathrm{T}} \boldsymbol{P}_{\widetilde{x}} \widetilde{\boldsymbol{x}}(k+i) \leqslant 1$, then $\widetilde{\boldsymbol{x}}(k+i+1)^{\mathrm{T}} \boldsymbol{P}_{\widetilde{x}} \widetilde{\boldsymbol{x}}(k+i+1) = \widetilde{\boldsymbol{x}}(k+i)^{\mathrm{T}} \boldsymbol{\Omega}^{\mathrm{T}} \boldsymbol{P}_{\widetilde{x}} \boldsymbol{\Omega} \widetilde{\boldsymbol{x}}(k+i) = \widetilde{\boldsymbol{x}}(k+i)^{\mathrm{T}} \boldsymbol{P}_{\widetilde{x}} \widetilde{\boldsymbol{x}}(k+i) \leqslant 1$, $i = 0, 1, 2, \ldots$. Moreover, if $\widehat{\boldsymbol{z}}(k+i|k)^{\mathrm{T}} \boldsymbol{P}_z \widehat{\boldsymbol{z}}(k+i|k) \leqslant 1$, then

$$\begin{aligned} &\widehat{\boldsymbol{z}}(k+i+1|k)^{\mathrm{T}} \boldsymbol{P}_z \widehat{\boldsymbol{z}}(k+i+1|k) \\ &= [\boldsymbol{\Theta} \widehat{\boldsymbol{z}}(k+i|k)^{\mathrm{T}} + \boldsymbol{\Psi} \widetilde{\boldsymbol{x}}(k)]^{\mathrm{T}} \boldsymbol{P}_z [\boldsymbol{\Theta} \widehat{\boldsymbol{z}}(k+i|k) + \boldsymbol{\Psi} \widetilde{\boldsymbol{x}}(k)] \\ &\leqslant \alpha_2 \widehat{\boldsymbol{z}}(k+i|k)^{\mathrm{T}} \boldsymbol{\Theta}^{\mathrm{T}} \boldsymbol{P}_z \boldsymbol{\Theta} \widehat{\boldsymbol{z}}(k+i|k) + \alpha_3 \widetilde{\boldsymbol{x}}(k)^{\mathrm{T}} \boldsymbol{\Psi}^{\mathrm{T}} \boldsymbol{P}_{\widetilde{x}} \boldsymbol{\Psi} \widetilde{\boldsymbol{x}}(k) \\ &\leqslant (1 - \alpha_1 \widetilde{x}_0) \widehat{\boldsymbol{z}}(k+i|k)^{\mathrm{T}} \boldsymbol{P}_z \widehat{\boldsymbol{z}}(k+i|k) + \alpha_1 \widetilde{\boldsymbol{x}}(k)^{\mathrm{T}} \boldsymbol{P}_{\widetilde{x}} \widetilde{\boldsymbol{x}}(k) \\ &\leqslant 1 - \alpha_1 \widetilde{x}_0 + \alpha_1 \widetilde{x}_0 = 1. \end{aligned}$$

The positive definite matrix $\boldsymbol{P}_z$ can then be rewritten as

$$\boldsymbol{P}_z = \begin{bmatrix} (\boldsymbol{P}_{11})_{m \times m} & \boldsymbol{P}_{12} \\ \boldsymbol{P}_{12}^{\mathrm{T}} & (\boldsymbol{P}_{22})_{Mp \times Mp} \end{bmatrix}.$$

Based on (14), we obtain

$$\widehat{\boldsymbol{x}}(k)^{\mathrm{T}} \boldsymbol{P}_{11} \widehat{\boldsymbol{x}}(k) \leqslant 1 - 2\boldsymbol{\xi}(k)^{\mathrm{T}} \boldsymbol{P}_{12}^{\mathrm{T}} \widehat{\boldsymbol{x}}(k) - \boldsymbol{\xi}(k)^{\mathrm{T}} \boldsymbol{P}_{22} \boldsymbol{\xi}(k). \tag{20}$$

Note that to maximize set $\mathcal{S}_{\widetilde{x}}$, the following optimization problem can be solved with $\boldsymbol{\xi}(k) = -\boldsymbol{P}_{22}^{-1} \boldsymbol{P}_{12}^{\mathrm{T}} \boldsymbol{x}(k)$ [27]:

$$\max_{\boldsymbol{\xi}(k)} \; 1 - 2\boldsymbol{\xi}(k)^{\mathrm{T}} \boldsymbol{P}_{12}^{\mathrm{T}} \widehat{\boldsymbol{x}}(k) - \boldsymbol{\xi}(k)^{\mathrm{T}} \boldsymbol{P}_{22} \boldsymbol{\xi}(k).$$

Then, with the optimal value $\boldsymbol{\xi}^*(k)$ of $\boldsymbol{\xi}(k)$ substituted into (20), a maximal set $\mathcal{S}_*$ can be obtained as follows:

$$\mathcal{S}_* = \{\widehat{\boldsymbol{x}}(k) | \widehat{\boldsymbol{x}}(k)^{\mathrm{T}} \boldsymbol{P}_* \widehat{\boldsymbol{x}}(k) \leqslant 1\}, \tag{21}$$

where $\boldsymbol{P}_* := \boldsymbol{P}_{11} - \boldsymbol{P}_{12}\boldsymbol{P}_{22}^{-1}\boldsymbol{P}_{12}^{\mathrm{T}} > 0$ [31]. When $\boldsymbol{\xi}(k) = 0$, we obtain $\boldsymbol{P}_x = \boldsymbol{P}_{11}$ from (11) and (20). Otherwise, $\boldsymbol{\xi}(k) \neq 0$, and we obtain $\boldsymbol{P}_* - \boldsymbol{P}_{11} \preceq 0$ as $\boldsymbol{P}_{12}$ and $\boldsymbol{P}_{22}^{-1}$ are both positive definite. Thus, $\boldsymbol{P}_x = \boldsymbol{P}_{11} \succeq \boldsymbol{P}_*$. Therefore, we have $\mathcal{S}_x \subseteq \mathcal{S}_*$, and the proposed method enlarges the allowable initial state set. Above all, we only need to maximize $\det(\boldsymbol{P}_*^{-1})$ such that the invariant set $\mathcal{S}_*$, which is proportional to $\det(\boldsymbol{P}_*^{-1})$, can be maximized.

Furthermore, using elementary row operations, $\boldsymbol{P}_z^{-1}$ can be solved as follows:

$$\boldsymbol{P}_z^{-1} = \begin{bmatrix} \boldsymbol{P}_{11} & \boldsymbol{P}_{12} \\ \boldsymbol{P}_{12}^{\mathrm{T}} & \boldsymbol{P}_{22} \end{bmatrix}^{-1} = \begin{bmatrix} (\boldsymbol{P}_{11} - \boldsymbol{P}_{12}\boldsymbol{P}_{22}^{-1}\boldsymbol{P}_{12}^{\mathrm{T}})^{-1} & * \\ * & * \end{bmatrix} = \begin{bmatrix} \boldsymbol{P}_*^{-1} & * \\ * & * \end{bmatrix}.$$

Because $\widehat{\boldsymbol{x}}(k) = \boldsymbol{F}\boldsymbol{z}(k)$ in (13), we obtain $\boldsymbol{P}_*^{-1} = \boldsymbol{F}\boldsymbol{P}_z^{-1}\boldsymbol{F}^{\mathrm{T}}$. Hence, the maximum invariant set $\mathcal{S}_*$ can be obtained by maximizing $\det(\boldsymbol{F}\boldsymbol{P}_z^{-1}\boldsymbol{F}^{\mathrm{T}})$, and the parameter design can be facilitated in the controller (9).

Now, to ensure the feasibility of the designed rotor-AMB control system, we present the following primary technical results.

Theorem 1. If Assumptions 1–3 hold, the asymptotical stability of the closed-loop rotor-AMB system composed of (6), (9), (16) and (17) can be guaranteed.

Proof. We assume that optimization problem (16) and (17) can be solved; then, from Assumption 2, $\boldsymbol{\xi}(k)$ always exists such that $\widehat{\boldsymbol{x}}(k+1) \in \mathcal{S}_*$ in (21) if $\widehat{\boldsymbol{x}}(k) \in \mathcal{S}_*$. At time $k+1$, a feasible choice for $\boldsymbol{\xi}(k+1)$ is given by $\widehat{\boldsymbol{\xi}}(k+1|k) = \boldsymbol{L}_2\boldsymbol{\xi}(k)$ according to (10). Because $\|\widehat{\boldsymbol{\xi}}(k+1|k)\|_2 = \|\boldsymbol{L}_2\boldsymbol{\xi}(k)\|_2 \leqslant \|\boldsymbol{L}_2\|_2\|\boldsymbol{\xi}(k)\|_2 = \|\boldsymbol{\xi}(k)\|_2$, a cost smaller than $J(k)$ is yielded by $\widehat{\boldsymbol{\xi}}(k+1|k)$.

However, $\widehat{\boldsymbol{\xi}}(k+1|k)$ may not always be the optimal result at the $(k+1)$-th step. The optimal cost $J^*(k+1)$ calculated at the $(k+1)$-th step with respect to the optimal solution $\boldsymbol{\xi}^*(k+1)$ is smaller than the cost $\widehat{J}(k+1|k)$ with respect to $\widehat{\boldsymbol{\xi}}(k+1|k)$. Hence, $J^*(k) \geqslant \hat{J}(k+1|k) \geqslant J^*(k+1)$, where $\hat{J}(k+1|k) = J^*(k)$ holds iff $\boldsymbol{\xi}(k+1) = 0$, and the two "=" s cannot exist simultaneously. Then, the optimal cost function $J^*(k)$ can be regarded as a Lyapunov function [29] which decreases with the increasing k.

It is noted that a sequence of $\hat{\boldsymbol{\xi}}(k+i|k) = \boldsymbol{L}_2\hat{\boldsymbol{\xi}}(k+i-1)$, $i = 1, 2, \ldots, M$ is generated by the dual-mode algorithm, which converges to zero within M steps. Hence, the system states can be included in the invariant set $\mathcal{S}_x$ in M steps or less. In this case, the asymptotic stability is guaranteed by the LQR control law (9) with $\hat{\boldsymbol{\xi}}(k|k) = 0$. The proof is thus completed.

The dual-mode algorithm is presented in Algorithm 1 in detail. In general, the set-point is established as $r(k) = 0$. Note that the calculation of the LMI offline is most time-consuming, and thus the complexity of the computation is substantially reduced.

Algorithm 1

Step 1. Calculate the LQR gain $\boldsymbol{K}$ (see Eq. (9)) and the observer $\boldsymbol{L}_1$ (see Eq. (8)) using the Kalman filter method;
Step 2. Set the predictive horizon M and the control constraint $\overline{u}$, and calculate the matrices $\boldsymbol{P}_z$ and $\boldsymbol{P}_{\widetilde{x}}$ based on Assumptions 1–3 using the YALMIP [32], while minimizing $-\log\det(\boldsymbol{F}\boldsymbol{P}_z^{-1}\boldsymbol{F}^{\mathrm{T}})$ with $\boldsymbol{F}$ given in Eq. (13);
Step 3. Set the value interval of the system state, calculate the optimal values $\boldsymbol{\xi}^*(k)$ based on (16) and (17), and iteratively establish a table Ξ of the optimal solutions for all the states;
Step 4. Obtain the current estimated state $\hat{\boldsymbol{x}}(k)$ at the k-th step;
Step 5. Select the optimal value $\boldsymbol{\xi}^*(k)$ from the table Ξ in step 3;
Step 6. Calculate the control law $\boldsymbol{u}(k)$ using (9), and then send the control signal to the rotor-AMB system;
Step 7. Continue to execute steps 4 to 6 until $\hat{\boldsymbol{x}}(k)$ converges to zero.

Remark 1. Extensive experiments show that Assumptions 1–3 are always feasible, if the control constraint $\overline{u} > 0$ is sufficiently large. The control effort and the settling time can be balanced by adjusting the weighting matrices $\boldsymbol{Q}$ and $\boldsymbol{R}$.

Remark 2. Using the MATLAB toolbox YALMIP [32], the matrix $\boldsymbol{P}_z$ can be calculated offline to minimize $-\log\det(\boldsymbol{F}\boldsymbol{P}_z^{-1}\boldsymbol{F}^{\mathrm{T}})$. Meanwhile, the optimal value $\xi^*(k)$ is computed offline based on the CVX method [33] in step 3, which forms the optimal solution table Ξ and balances the online computation time and the control effect. Moreover, to balance the allowable initial state region, a suitable prediction horizon M must be selected, which will be described in Section 4.

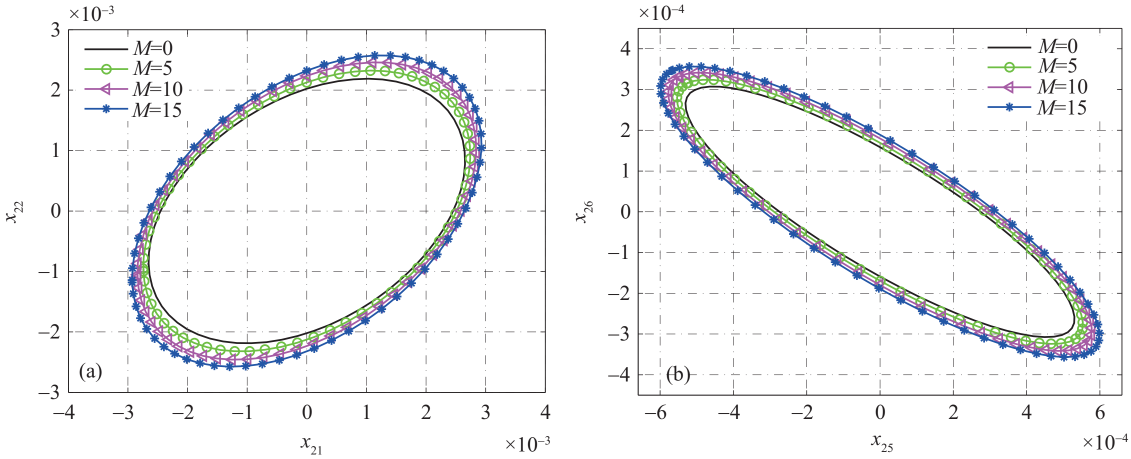

Figure 3 (Color online) The super-ellipsoidal invariant set $\mathcal{S}_*$ (see Eq. (21)) of the AMB system increases as the prediction step M increases. (a) and (b) display projections of the set $\mathcal{S}_*$ onto the x_{21}-x_{22} and x_{25}-x_{26} planes, respectively. Meanwhile, $M = 0$ represents the conventional LQR control (i.e., $\xi(k) = 0$).

4 Experiments

Accordingly, we performed suspension control experiments on two radial AMBs. The model parameters are listed in Table 1. Therein, the subscripts f and b indicate the front and back parameters for the AMB, respectively. To address larger deviations, which are often encountered in practical applications, the feedback controller is expected to enlarge the region of attraction $\mathcal{S}_*$ (see Eq. (21)). Thus, in Figure 3, we present the attraction $\mathcal{S}_*$ regions for the LQR method and the MPC method, respectively. However, it is difficult to plot the entire hyper-ellipsoidal attraction region for a 36-dimensional space; thus, the projections of $\mathcal{S}_*$ onto the x_{21}-x_{22} and x_{25}-x_{26} planes are displayed in Figures 3(a) and (b). Note that the attraction region expands as the prediction step M increases. However, selecting a large M may result in a high computational complexity for (16) and (17); thus, we select $M = 15$ to ensure that the computational complexity and initial state region are balanced.

First, we can calculate the LQR gain matrix $\boldsymbol{K}$ for two AMBs in MATLAB, in which the pre-set matrices $\boldsymbol{Q} \in \mathbb{R}^{36}$ and $\boldsymbol{R} \in \mathbb{R}^{4}$ can be set as diagonal matrices, with the diagonal elements selected from $(0, q)$ and $(0, r)$, respectively. Meanwhile, the term $\boldsymbol{\xi}(k)$ in (9) is obtained by choosing a suitable predictive horizon M. It is worth mentioning that the present control algorithm is executed in the FPGA/VHDL program. Thus, our method is simply programmed when the actual model is approximated by the ideal model. Thereby, we represent the MPC controller by a matrix of control values derived via MATLAB.

Next, our algorithm is compiled with FPGA using the controller parameters as follows: $\overline{u} = 0.5$, $\alpha_1 = 1.3$, $\alpha_2 = 1.27$, $\widetilde{x}_0 = 0.002$, $M = 15$. Meanwhile, we set a suitable external condition, i.e., a supply voltage of 60 V, to drive the amplifier circuit. Figure 4 indicates that the proposed controller effectively reduces the settling time of the rotor-AMB with control input constraints, and the settling time and tracking error are reduced by 34.6% and 21.6%, respectively. More precisely, the proposed DMPC has a shorter settling time and a smaller steady-state tracking error (see Figures 4(a) and (b)), and the activation period of the input constraint is shorter than that of the LQR due to its superior ability in handling input constraints (see Figures 4(c) and (d)). To more clearly demonstrate the control performance, we depict the rotor's suspension track in x-y-t space, as shown in Figure 5. Therein, both trajectories converge to the center point (i.e., the rotors are levitated). Both the settling time and tracking error of the proposed method are smaller than those of LQR; thus, the superiority of the presented method is verified.

To compare the vibration mitigation performances for the LQR and DMPC, a random machine loading disturbance is added to the displacement signal by controller a_2 (see Figure 2), which is a decreasing random interference signal generated by a software (continuous 19.5 ms), as shown in Figures 6(a) and (b). Both controllers mitigate the vibrations, as shown in Figures 6(c) and (d), and the DMPC scheme

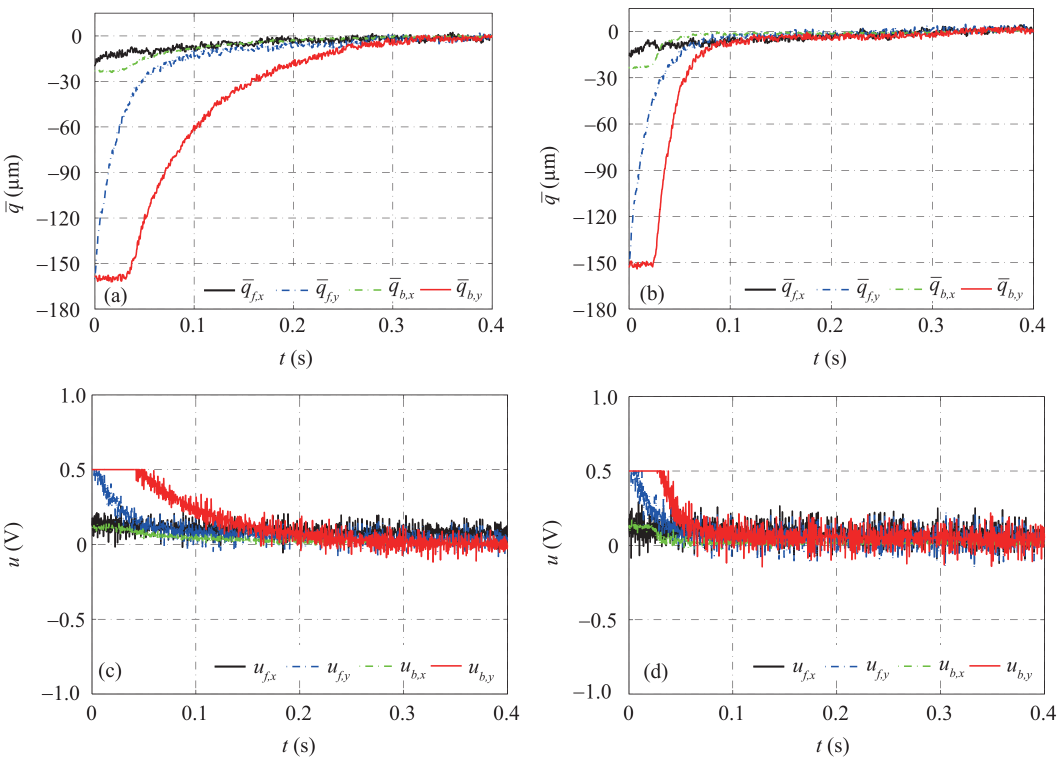

Figure 4 (Color online) The rotor-AMB closed-loop suspension control, with a comparison between the conventional LQR method (a), (c) and DMPC method (b), (d). (a), (b) and (c), (d) display the output and input evolutions of the rotor-AMB closed-loop system during the suspension process, respectively.

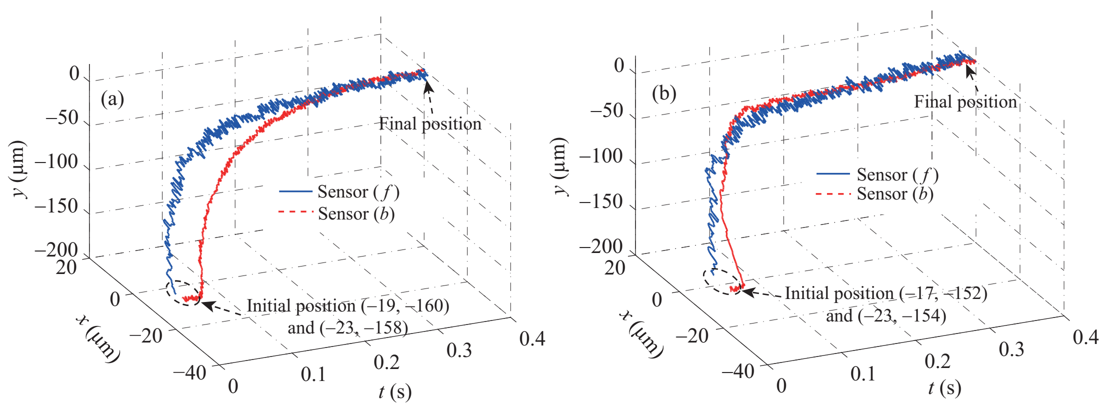

Figure 5 (Color online) Moving trajectories in the x-y plane for the suspension procedure of the rotor measured by the front and back position sensors, respectively. (a) Conventional LQR; (b) DMPC.

has a much shorter settling time and smaller response oscillations in the expanded area of stability. The performance of the designed controller indicates that the system exhibits superior stabilization for external re-occurring forces. Thus, the effectiveness of the designed control method has been verified, and the rotor-AMB system exhibits a more robust performance way with DMPC than with LQR.

5 Conclusion

In this paper, a dual-mode predictive suspension control scheme is proposed for the rotor-AMB system with input constraints. This scheme can stably levitate the rotor and mitigate the vibrations excited by external disturbances in a closed-loop rotor-AMB system. A technical stability analysis is performed to

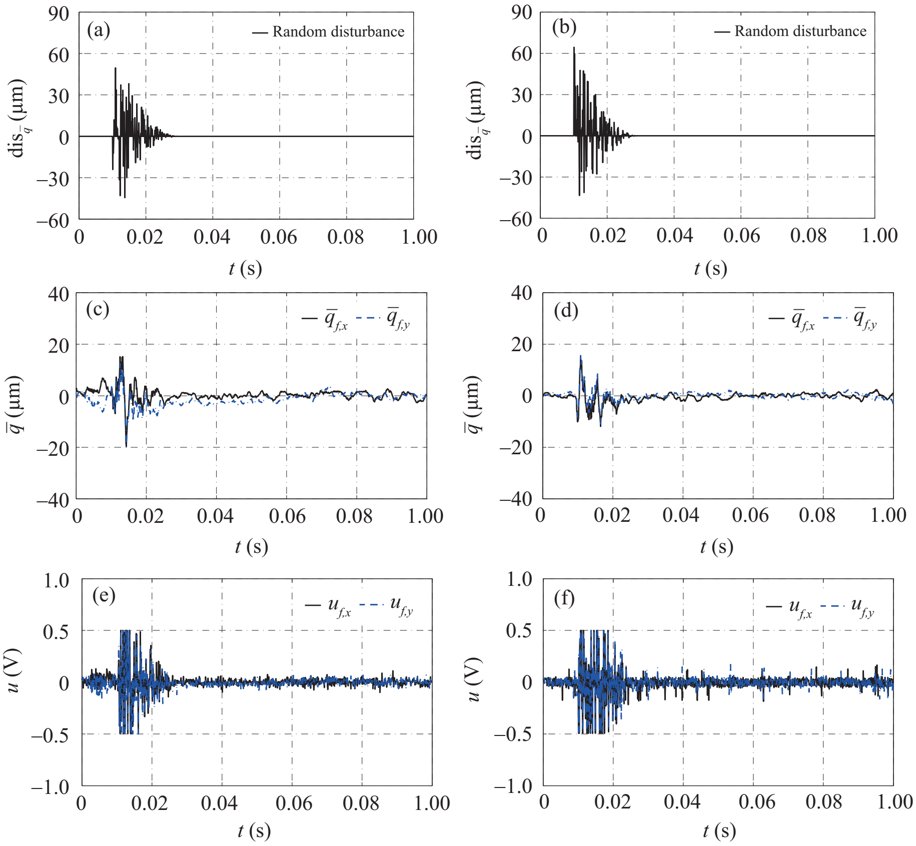

Figure 6 (Color online) Comparison of the vibration control performance for the conventional LQR method (a), (c), (e) and the proposed DMPC method (b), (d), (f). (a), (b) present the random disturbances manually added to the rotor; (c), (d) and (e), (f) display the corresponding output and input, respectively.

derive feasible conditions for the designed MPC method. Extensive levitation experiments validate the superiority of the method proposed in this paper.

Acknowledgements This work was supported by National Natural Science Foundation of China (Grant Nos. U1713203, 61803168, 51729501) and China Postdoctoral Science Foundation (Grant No. 2018M642822).

References

1 Knospe C R. Active magnetic bearings for machining applications. Control Eng Pract, 2007, 15: 307–313
2 Lim T M, Zhang D, Yang J, et al. Design and parameter estimation of hybrid magnetic bearings for blood pump applications. Mech Syst Signal Process, 2009, 23: 2352–2382
3 Fittro R L, Knospe C R. μ control of a high speed spindle thrust magnetic bearing. In: Proceedings of IEEE International Conference on Control Applications, 1999. 570–575
4 Zhang L, Liu K. Riccati difference equation in optimal control for magnetic bearings. Sci China Technol Sci, 2012, 55: 2107–2114
5 Schweitzer G, Maslen E H. Magnetic Bearings: Theory, Design, and Application to Rotating Machinery. Berlin: Springer, 2009
6 Maslen E H, Sawicki J T. μ-synthesis for magnetic bearings: why use such a complicated tool? In: Proceedings of ASME 2007 International Mechanical Engineering Congress and Exposition, 2007. 1103–1112
7 Sivrioglu S. Adaptive control of nonlinear zero-bias current magnetic bearing system. Nonlinear Dyn, 2007, 48: 175–184
8 Kang M S, Lyou J, Lee J K. Sliding mode control for an active magnetic bearing system subject to base motion. Mechatronics, 2010, 20: 171–178
9 Kuseyri I S. Robust control and unbalance compensation of rotor/active magnetic bearing systems. J Vib Control, 2012, 18: 817–832
10 Dong L L, You S L. Adaptive control of an active magnetic bearing with external disturbance. ISA Trans, 2014, 53: 1410–1419
11 Pesch A H, Smirnov A, Pyrhonen O, et al. Magnetic bearing spindle tool tracking through μ-synthesis robust control. IEEE/ASME Trans Mechatron, 2015, 20: 1448–1457

12 Kandil M S, Dubois M R, Bakay L S, et al. Application of second-order sliding-mode concepts to active magnetic bearings. IEEE Trans Ind Electron, 2018, 65: 855–864

13 Xie J, Zeng X J, Zhang M M, et al. Implementation of active magnetic control system for piston centering in labyrinth piston compressor. Mechatronics, 2018, 54: 52–67

14 Chen M, Wu Q X, Jiang C S, et al. Guaranteed transient performance based control with input saturation for near space vehicles. Sci China Inf Sci, 2014, 57: 052204

15 Chen M, Ren B B, Wu Q X, et al. Anti-disturbance control of hypersonic flight vehicles with input saturation using disturbance observer. Sci China Inf Sci, 2015, 58: 070202

16 Albin T. Benefits of model predictive control for gasoline airpath control. Sci China Inf Sci, 2018, 61: 070204

17 Harinath E, Foguth L C, Braatz R D. A robust dual-mode MPC approach to ensuring critical quality attributes in quality-by-design. In: Proceedings of American Control Conference (ACC), 2016. 2041–2046

18 Yuan Y, Zhang H T, Wu Y, et al. Bayesian learning-based model-predictive vibration control for thin-walled workpiece machining processes. IEEE/ASME Trans Mechatron, 2017, 22: 509–520

19 Cai Z, Haq A A U, Cholette M E, et al. Energy efficiency and tracking performance evaluation for dual-mode model predictive control of HVAC systems. J Thermal Sci Eng Appl, 2018, 10: 041023

20 Maciejowski J M. Predictive Control: With Constraints. Englewood Cliffs: Prentice Hall, 2002

21 Ruan X G, Hou X Y, Ma H Y. Stability analysis of constrained MPC with CLF applied to discrete-time nonlinear system. Sci China Inf Sci, 2014, 57: 112201

22 Zhang Y Y, Cao W H, Jin Y L, et al. An ensemble model based on weighted support vector regression and its application in annealing heating process. Sci China Inf Sci, 2019, 62: 049202

23 Mayne D Q, Rawlings J B, Rao C V, et al. Constrained model predictive control: stability and optimality. Automatica, 2000, 36: 789–814

24 Guo L L, Gao B Z, Li Y, et al. A fast algorithm for nonlinear model predictive control applied to HEV energy management systems. Sci China Inf Sci, 2017, 60: 092201

25 Zhang H, Wang T, Zhao Y L. FIR system identification with set-valued and precise observations from multiple sensors. Sci China Inf Sci, 2019, 62: 052203

26 Zhang H T, Wu Y, He D, et al. Model predictive control to mitigate chatters in milling processes with input constraints. Int J Mach Tools Manu, 2015, 91: 54–61

27 Kouvaritakis B, Rossiter J A, Schuurmans J. Efficient robust predictive control. IEEE Trans Autom Control, 2000, 45: 1545–1549

28 Zhang H T, Li H X, Chen G. Dual-mode predictive control algorithm for constrained Hammerstein systems. Int J Control, 2008, 81: 1609–1625

29 Khalil H K. Nonlinear Systems. Englewood Cliffs: Prentice Hall, 2012

30 Zhang H T, Chen G, Chen M Z Q. A novel dual-mode predictive control strategy for constrained Wiener systems. Int J Robust Nonlinear Control, 2009, 20: 975–986

31 Zhang F Z. The Schur Complement and Its Applications. Berlin: Springer, 2006

32 Lofberg J. YALMIP: a toolbox for modeling and optimization in matlab. In: Proceedings of IEEE International Conference on Robotics and Automation, 2004. 3753–3757

33 Blondel V D, Boyd S P, Kimura H. Recent Advances in Learning and Control. Berlin: Springer, 2008